Tribol Lett (2012) 48:407–415
DOI 10.1007/s11249-012-0021-x

ORIGINAL PAPER

Fabrication and Tribological Investigation of a Novel Hydrophobic Polydopamine/Graphene Oxide Multilayer Film

Junfei Ou · Lei Liu · Jinqing Wang · Fajun Wang · Mingshan Xue · Wen Li

Received: 17 March 2012 / Accepted: 23 July 2012 / Published online: 5 September 2012

Abstract Polydopamine (PDA)/graphene oxide (GO) multilayer was successfully constructed on the surface of silicon substrate by a layer-by-layer self assembling process. In order to further obtain hydrophobic outer surface, low energy molecules of 1H, 1H, 2H, 2H-perfluorodecyltrichlorosilane (PFDTS) were grafted thereon and the sample was coded as PDA/GO-PFDTS. The microstructures, chemical compositions, and morphologies of PDA/GO-PFDTS were characterized by the water contact angle (WCA) measurements, Fourier transform infrared spectroscopy (FTIR), X-ray photoelectron spectroscopy (XPS), and atomic force microscopy (AFM). In particular, the tribological performances were investigated by AFM and ball-on-plate tribometer. Experimental results showed that PDA/GO-PFDTS could lower the stiction and friction greatly as compared with the bare substrate and control samples. It was indicated that the as-fabricated film of PDA/GO-PFDTS was a very promising candidate for solving the tribological problems in micro/nano devices.

Keywords Layer-by-layer self assembly · Graphene oxide · Polydopamine

J. Ou · F. Wang · M. Xue · W. Li (✉)
School of Materials Science and Engineering, Nanchang Hangkong University, Nanchang 330063, People's Republic of China
e-mail: wenl@ualberta.ca

L. Liu
Institute of Pharmaceutics, Pharmaceutical College, Henan University, Kaifeng 475004, People's Republic of China

J. Wang
State Key Laboratory of Solid Lubrication, Lanzhou Institute of Chemical Physics, Chinese Academy of Sciences, Lanzhou 730000, People's Republic of China

1 Introduction

Recently, graphene oxide (GO) has become a hot topic not only for its low cost and mass production but also for its well dispersion in solvent (such as water) and further chemical modification/reduction. Based on these features, some factors restricting the development of graphene can be relieved.

For example, one restricting factor is that graphene is difficult to be transferred onto solid substrates with strong adhesion due to its lack of functional groups; however, based on their well dispersion in solvent and functional groups, GO sheets can be easily mounted onto solid substrates by solution-based techniques [1–4] and further be reduced or chemically modified. In order to further enhance the interfacial bonding strength, substrates with special properties (charged [5, 6]) or chemical composition (amine outer groups [7, 8]) are generally required. For instance, in our recent works, GO and reduced GO (rGO) sheets were assembled onto the silicon wafer pre-modified by self-assembled monolayers of 3-aminopropyl triethoxysilane with amine tail groups [7, 8]. However, it still remains a challenge to fabricate graphene-based multilayer by such methods.

Recently, due to its prominent advantages, such as the simplicity, universality, and thickness control at the nano-scale level, layer-by-layer (LBL) self-assembly technique has been introduced to fabricate such graphene-based multilayer [9–13]. For example, based on sequential adsorption of oppositely charged molecules (e.g., poly-electrolyte and oxide sheets) and chemically modified rGO, graphene-based film on silicon or glass slides have been constructed [14, 15]. These pioneer works have set good examples for electrostatic LBL assembling of graphene-based architectures. In this work, a new non-electrostatic LBL (NELBL) assembling process is proposed to construct

GO multilayers. Besides the component of GO sheets, the newly reported dopamine molecules are selected as the building block, which can be adsorbed onto almost all material surfaces and undergo oxidation-polymerization to form polydopamine (PDA) layer; [16] more importantly, PDA is abundant with reactive surface groups such as amine and hydroxyl groups [17]. Taking these advantages, a non-electrostatic LBL assembling process can be performed (schematically shown in Fig. 1).

As revealed in our recent work, GO and rGO sheets were found to possess good anti-wear resistance [7, 8]. Herein, the purpose of constructing this PDA/GO multilayer is also to reveal its potential application as lubricant film in nanodevices such as micro- and nano-electromechanical systems (MEMS/NEMS). It is commonly recognized that a hydrophobic outer surface is quite necessary for lubricant film to control the stiction in MEMS/NEMS [18]. In order to construct such hydrophobic outer surface, fluoroalkylsilane molecules of 1H, 1H, 2H, 2H-perfluorodecyltrichlorosilane (PFDTS) were grafted onto the surface of PDA/GO multilayer and the consequent film was labeled as PDA/GO-PFDTS. The tribological properties of the developed multilayer film of PDA/GO-PFDTS were evaluated and compared with the controlled samples. It is expected that the as-prepared PDA/GO-PFDTS may find wide applications as lubricant films in MEMS/NEMS not only for the excellent tribological behaviors of GO sheets but also for the unique multilayer architectures.

2 Experimental

2.1 Materials and Reagents

Expandable graphite was obtained from Qingdao Hensen Graphite Co., Ltd. 3-Hydroxytyramine hydrochloride (Dopamine hydrochloride, 99 %), 3-aminopropyl triethoxysilane (APTES, 99 %), and tris(hydroxymethyl) aminomethane (TRIS, 99.8 %) were purchased from Acros Organics; 1H, 1H, 2H, 2H-perfluorodecyltrichlorosilane (PFDTS, 96 %) was purchased from Alfa Aesar. All other reagents were analytical grade and used as received. The P-type polished single-crystal Si (111) wafer was obtained from GRINM Semiconductor Materials Co. (Beijing,

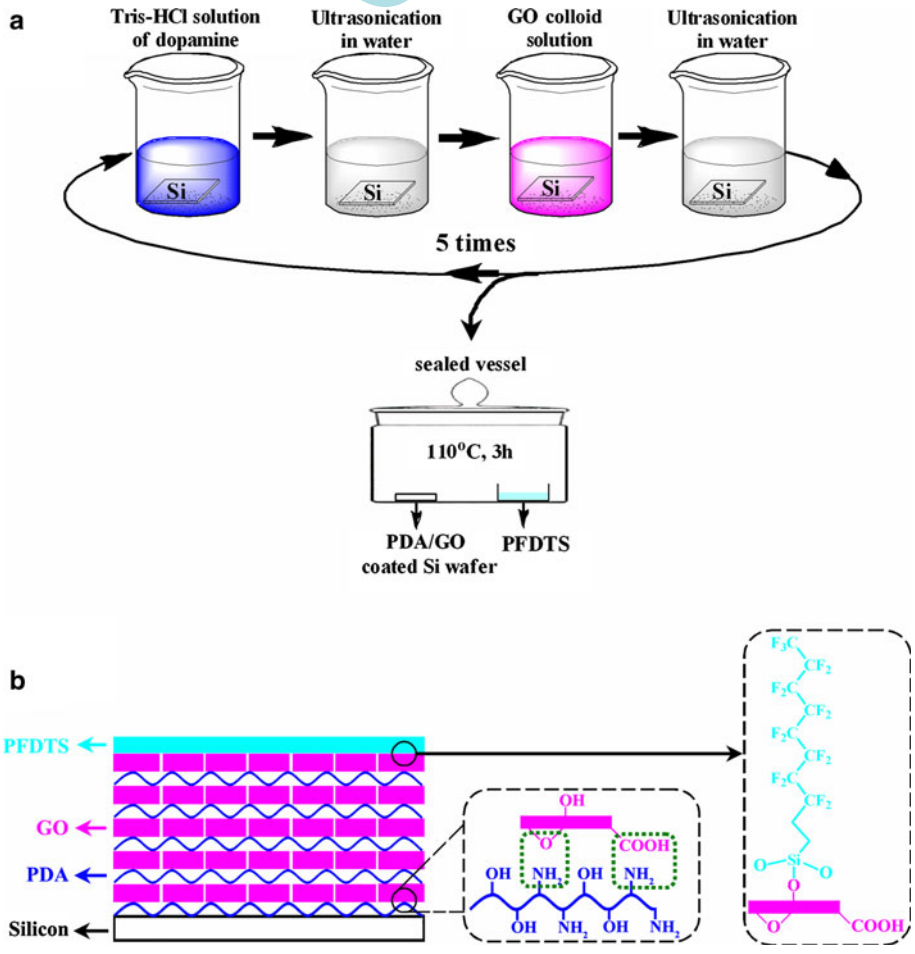

Fig. 1 Procedures to fabricate PDA/GO-PFDTS (**a**); proposed microstructure and possible interlayer interaction of the film (**b**)

China). Ultrapure water (>18 MΩ cm) was used in this work.

2.2 Preparation of GO Colloid Solution

Expandable graphite was first heated at 1,050 °C in air for 15 s. The heat-treated expandable graphite powder (1 g) was then added to 98 % H_2SO_4 (23 mL) in an ice bath with stirring, and $KMnO_4$ (3 g) was subsequently added slowly. The mixture was kept at 35 °C in a water bath for 30 min. Ultrapure water (46 mL) was gradually added, and the mixture was immersed in ice water. After 15 min, the mixture was further treated with ultrapure water (140 mL) and 30 % H_2O_2 solution (12.5 mL). The obtained mixture was first washed with ultrapure water until a pH level of 7 was reached, and was then dialyzed with stirring until SO_4^{2-} anions could no longer be detected by the $BaCl_2$ solution (1 M). A diluted GO colloid solution with a concentration of 0.4 mg mL^{-1} was employed in the succeeding process.

2.3 Fabrication of PDA/GO-PFDTS and the Controlled Samples

Silicon wafers were cleaned in a piranha solution (a mixture of 7:3 (v/v) 98 % H_2SO_4 and 30 % H_2O_2) at 90 °C for 30 min. After being thoroughly rinsed with ultrapure water and blown dry with N_2, the silicon wafers were immersed into a TRIS–HCl buffer solution (25 mL, 10 mM, pH 8.5) of dopamine (0.05 g) for 1 h. Then, the sample was taken out to clean in ultrapure water by ultrasonication and blown dry with N_2. Subsequently, the sample was kept in GO aqueous solution at 80 °C for 1 h followed by an ultrasonication and blow-drying process. The sequential immersion in dopamine and GO colloid solution resulted in the formation of PDA/GO multilayer. Then, PFDTS molecules were deposited onto the surface of PDA/GO by a chemical vapor deposition (CVD) process. Specifically, PDA/GO was introduced into a sealed vessel with a container containing 20 μL PFDTS and maintained at 110 °C for 3 h. Finally, the samples were ultrasonicated in toluene, acetone, and ultrapure water in turn to remove the physisorbed molecules. The whole process was schematically shown in Fig. 1.

The controlled samples without GO sheets, i.e., PDA and PDA-PFDTS were prepared via the similar process by omitting the immersion into the GO colloid solution. We also tried to fabricate a sample without PDA component by the similar procedure by omitting the immersion into dopamine buffer solution; however, due to the absence of adhesive PDA layer, it failed. Self-assembled monolayers of PFDTS (coded as PFDTS-SAMs) were prepared on Si substrate by the above-mentioned CVD process. The tribological properties of the controlled samples (PDA, PDA-PFDTS, and PFDTS) were tested and compared with the samples of PDA/GO and PDA/GO-PFDTS.

2.4 Characterizations

Attenuated total reflectance Fourier transform infrared (ATR-FTIR) spectra were recorded with an IFS 66 V/S FTIR spectrometer (Bruker, Germany) using a Harrick Scientific horizontal reflection Ge-attenuated total reflection accessory (GATR, incidence angle 65°). In order to eliminate the effect of H_2O and CO_2, the pressure in the sample chamber and optical chamber was kept below 6.0×10^{-4} MPa.

X-ray photoelectron spectroscopy (XPS, PHI-5702, Physical Electronics, USA) was performed using a monochromated Al-Kα irradiation. The chamber pressure was about 3×10^{-8} Torr under testing condition. Peak deconvolution and quantification of elements were accomplished using the software of Origin 7.0.

Water contact angle (WCA) of different samples was determined using a DSA100 contact angle meter (Krüss, Germany). The averaged values of at least five repeat measurements for each sample were obtained.

The surface morphologies of different samples were observed by a Nanoscope IIIa multimode atomic force microscope (AFM, Veeco, USA) in tapping mode. The micro-tribological properties of different film samples were measured using the same AFM in contact mode. Triangular silicon nitride cantilevers with a normal force constant of 2 N m^{-1} were employed for AFM measurements. No attempt was made to calibrate the torsional force constant, and the same cantilever was applied in all measurements. The output voltages were directly used as the relative frictional force. A series of measurements of friction-load relationship was conducted from friction loops obtained from at least five separate locations on each sample surface. In order to obtain the adhesive force between the AFM tip and the film surface, the force-distance curve was recorded on a CSPM 4000 AFM (Being Nano-Instrument, China). The pull-off force was considered as the adhesive force. All experiments were carried out under ambient conditions of 20 °C and 30 % relative humidity.

Macro-tribological tests were run on an UMT-2MT tribometer (CETR, USA) in a ball-on-plate contact configuration. Commercially availed steel balls ($\varphi = 3$ mm, announced mean roughness = 0.02 μm) were used as the stationary upper counterparts, while the lower tested samples were mounted onto the flat base and driven to reciprocally slide at a distance of 0.5 cm. The friction coefficient-versus-time curves were recorded automatically. At least three repeat measurements were performed for each frictional pair. The friction coefficient and anti-

wear life were measured at a relative error of ±10 and ±5 %, respectively.

3 Results and Discussion

3.1 Formation and Characterization of PDA/GO-PFDTS

PDA/GO-PFDTS film was constructed by mainly two steps: NELBL self assembling of PDA/GO multilayer and the chemo-grafting of PFDTS thereon. As shown in Fig. 1a, the fabrication procedure is quite simple. However, compared with the simple process, the driving force for such NELBL self assembling seems to be a mystery. In order to reveal such driving force, it is quite necessary to know the basic chemical nature and reactivity of the components, i.e., GO sheets and PDA. It is well known that GO is a graphite derivative with covalently attached oxygen-containing groups (such as epoxy, carboxyl, and hydroxyl groups; Fig. 1b) [19–21]. As reported by Niu et al. and verified in our recent studies, the epoxy and carboxyl group of GO can react with the amine group of APTES molecules [7, 22]. Meanwhile, PDA, the other component for the multilayer, has two characteristics: high adhesion to substrates and highly reactive due to the active surface groups (such as hydroxyl and amine) [16]. So, the driving force for such LBL in this work was supposed to be a series of surface reactions between the functional groups of PDA and GO.

In order to clarify such reactions, ATR-FTIR and XPS spectra for different samples were recorded. As shown in Fig. 2, for PDA, the peaks located at 2,926/2,852 and 1,457–1,595 cm^{-1} emerged, which were ascribed to CH_2 and benzene ring moiety in dopamine molecules,

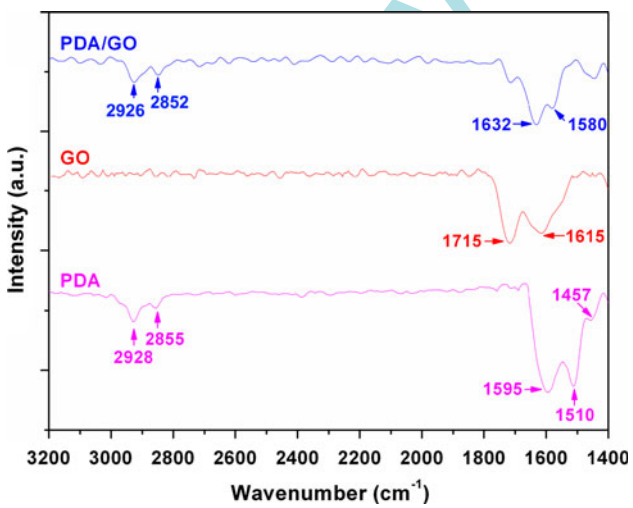

Fig. 2 ATR-FTIR spectra of different samples

respectively. For GO, signals at 1,715 and 1615 cm^{-1} were ascribed to the C=O stretching of carboxyl and O–H bending of C–OH, respectively. After incorporation to form PDA/GO multilayer, apparent peaks at 1,632 and 1,580 cm^{-1} appeared, which were typical signals for amido or zwitterionic $COO–NH_3^+$ linkages. However, considering the absence of a coupling agent such as 1-ethyl-3-(3-dimethylaminopropyl)-carbodiimide (EDC), the latter was more likely to be formed.

The fabrication of PDA/GO-PFDTS was monitored by XPS. The survey spectra for PDA on silicon substrate were depicted in Fig. 3a. It is apparent that besides the signals for carbon and oxygen elements, *N 1s* peak (399.9 eV) emerged. After incorporation with GO and further grafted with PFDTS, the *N 1s* peak at 399.8 eV was still visible (Fig. 3b). Compared with PDA or GO, an obvious change after incorporation for the sample of PDA/GO is the disappearance of *Si 2s* and *Si 2p* signals. This is because the film gets thick as the assembling progressed and the photoelectron can not reach the substrate. Thus, the signals ascribed to the substrate vanished for PDA/GO and PDA/GO-PFDTS. *C 1s* spectra for PDA, GO, PDA/GO, and PDA/GO-PFDTS were given in Fig. 3d–g. *C 1s* of PDA (Fig. 3d) was deconvoluted into three components with binding energy at 284.7 eV (C–C in the benzene ring), 286.1 eV (C–O and C–N), and 288.1 eV (C=O in the structure of dopaminequinone) [23–26]. Similarly, *C 1s* of GO was deconvoluted into four components with binding energy at 284.6, 285.8, 287.1, and 288.9 eV, which were attributed to the C–C, C–O, C=O, and OH–C O species, respectively (Fig. 3e) [7, 27]. After incorporation with each other to form a PDA/GO film, the signals for C–C (284.7 eV), C–O/C–N (286.0), C=O (287.1), and OH–C=O (288.7 eV) were still visible (Fig. 3f). Moreover, the content of non-oxygenated carbon (C–C) for PDA/GO (61.1 %) was lower than that of PDA (71.0 %) and higher than that of GO (52.5 %). After grafted with PFDTS, characteristic peak of *F 1s* at 688.8 eV appeared (Fig. 3a, c). Correspondingly, a signal at 291.4 eV ascribed to C–F bond emerged in *C 1s* spectrum of PDA/GO-PFDTS (Fig. 3g) [28].

WCA measurement is a simple, useful, and sensitive tool to gain insights into the chemical nature of material surface. The variation of WCA for PDA/GO multilayer is depicted in Fig. 4. Obviously, WCA varied regularly as a result of the alternate deposition of the PDA and GO layer. WCA for PDA is 54.9°, well consistent with the value reported in the literatures [16, 29, 30]. Upon the completion of GO deposition, WCA decreases to about 39.6°. After grafted with PFDTS, WCA increases sharply to 105 (±1.4)°, which is close to that of PDA-PFDTS (102.3 ± 1.4°) but still a little lower than that of PFDTS-SAMs on Si substrate (109 ± 1.5°). This difference is most

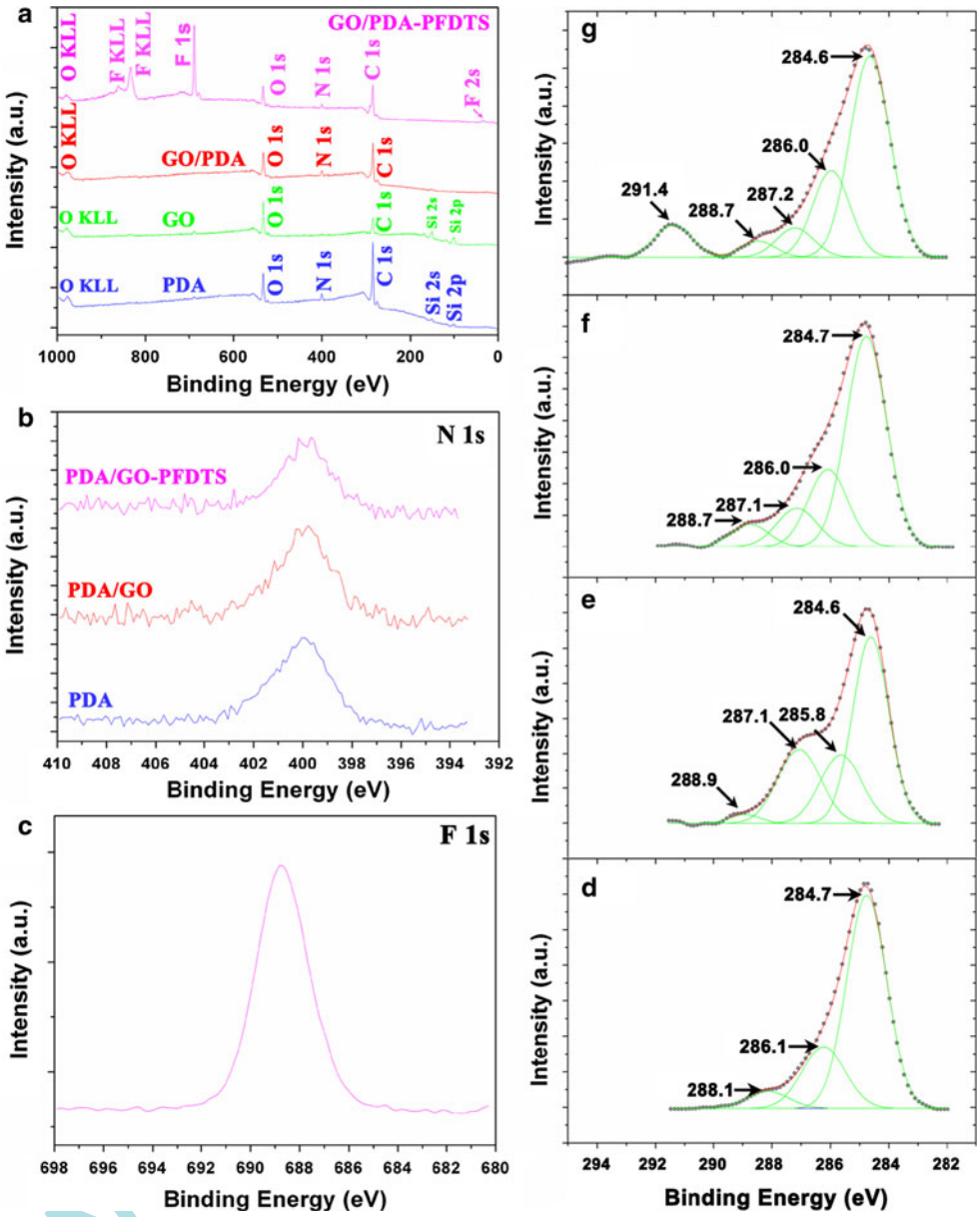

Fig. 3 XPS survey spectra for different samples (**a**); *N 1s* spectra for different samples (**b**); *F 1s* for PDA/GO-PFDTS (**c**); *C 1s* spectra for PDA (**d**), GO (**e**), PDA/GO (**f**), and PDA/GO-PFDTS (**g**)

likely due to the distinct chemical nature of the sublayer. In other words, compared with the PDA/GO or PDA sublayer, it is expected that the hydroxylated Si substrate is abundant with more surface hydroxyl groups, which are the reactive points to induce the self assembling of PFDTS. Consequently, PFDTS on bare Si substrate tends to pack more densely and yield a higher WCA.

AFM morphologies of GO sheets and PDA on Si substrates have been well discussed in our previous studies [7, 8, 29]. Herein, to obtain further information about the surface microstructures of PDA/GO and PDA/GO-PFDTS, samples were examined by AFM in tapping mode. As shown in Fig. 5a, GO sheets were still faintly visible after incorporated with PDA. Under larger magnification (Fig. 5b), nanoparticles with diameter of 30 nm were observed, which were ascribed to the deposited PDA component. After grafted with PFDTS, GO sheets were not so easy to differentiate from the matrix (Fig. 5c), while the nanoparticles at larger magnification were still clearly visible (Fig. 5d).

3.2 Adhesive and Nano-Tribological Investigation

Due to the large surface-to-volume ratio of MEMS/NEMS, surface force such as adhesion and friction increased greatly. Consequently, two major design limitations, i.e., stiction and wear, emerged. It was widely observed that a hydrophobic nanofilm, such as self-assembled monolayers/multilayers, could reduce such surface forces [31]. In order to estimate the anti-stiction and wear-resistant behaviors,

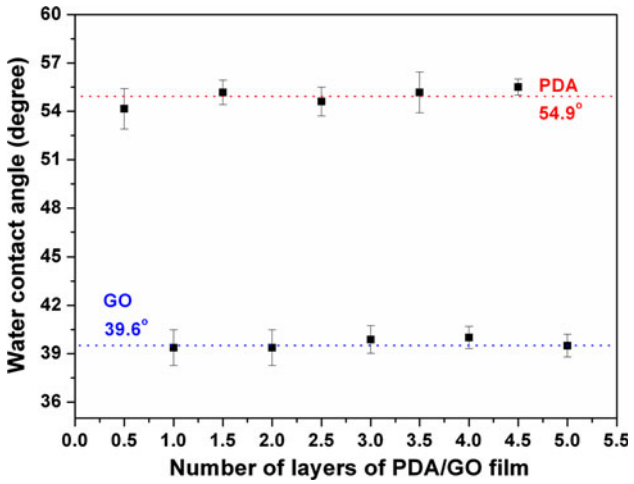

Fig. 4 WCA of the PDA/GO multilayer films as a function of the layer number

the adhesive (Fig. 6a) and micro/macro-tribological (Figs. 6b, 7) performances were investigated.

As depicted in Fig. 6a, strong adhesion of 152.5 nN was observed on PDA/GO surface. Once PFDTS was generated thereon, the adhesive force reduced to 60.8 nN. Similar variation was also observed for the sample pair of hydroxylated Si (201.7 nN)/PFDTS-SAMs (57.8 nN) and PDA (130.5 nN)/PDA-PFDTS (62.4 nN). It can be concluded that the adhesive force for the hydrophilic samples (i.e., hydroxylated Si substrate, PDA, and PDA/GO) is in a high level; after grafted with PFDTS (i.e., PFDTS-SAMs, PDA-PFDTS, and PDA/GO-PFDTS), adhesive force decreases correspondingly. This obvious variation can be attributed to the change in the hydrophobicity of the surfaces. In other words, the adhesive force is greatly suppressed with increasing hydrophobicity of the surface. Such phenomenon indicates that PFDTS outer layer can obviously lower interfacial energy on silicon wafer and the capillary force between the tip and surface [28].

The nano-scale friction force-versus-applied load curves measured in an AFM are depicted in Fig. 6b. It is obvious that these curves can be fitted by straight lines. There are two important parameters for such lines, i.e., the slope ($\partial y/\partial x$) and the intercept. The former is generally viewed as friction coefficient. However, as shown in Fig. 6b, the Y axis (frictional force signal) is expressed in raw voltage signal. So, the slope can just be taken as a "relative coefficient of friction" (RCF) to compare with each other to evaluate the lubricity [7, 8]. Based on the magnitude of RCF, the tested samples can be roughly divided into two groups, i.e., hydrophilic and hydrophobic ones. For hydrophilic ones, RCF is in a high level. It can be seen from Fig. 6b that the hydroxylated silicon wafer records a highest RCF of 2.25, which decreases slightly to 1.96 or

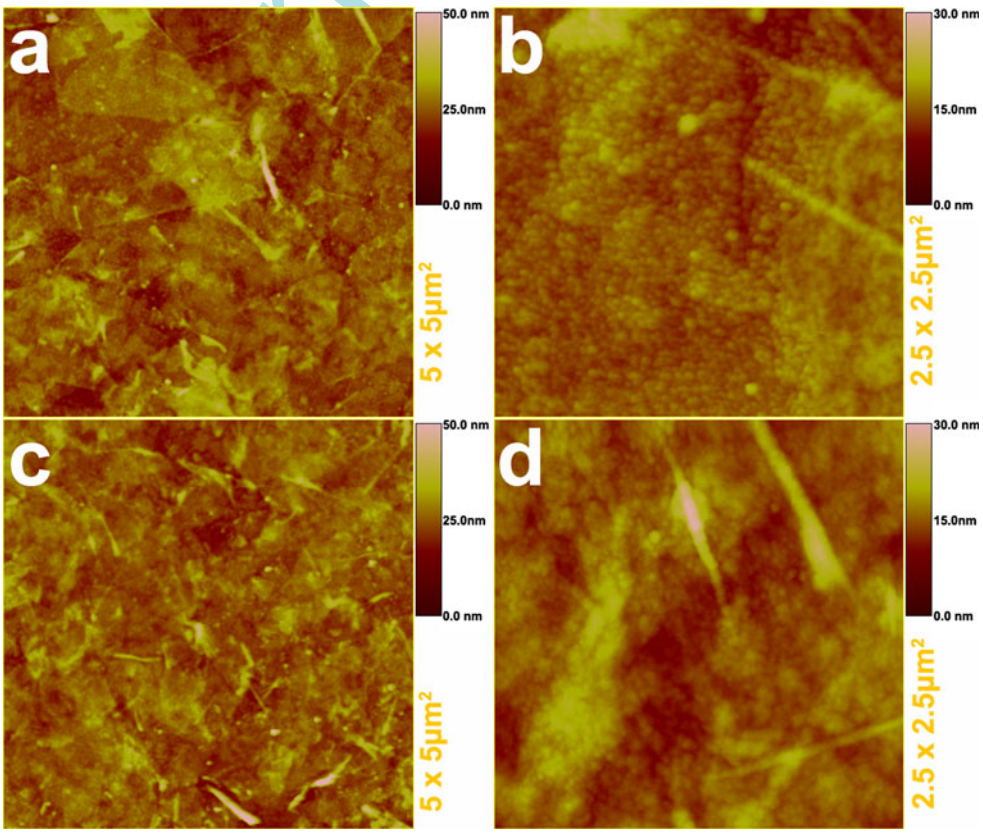

Fig. 5 AFM images of PDA/GO (**a**, **b**) and PDA/GO-PFDTS (**c**, **d**)

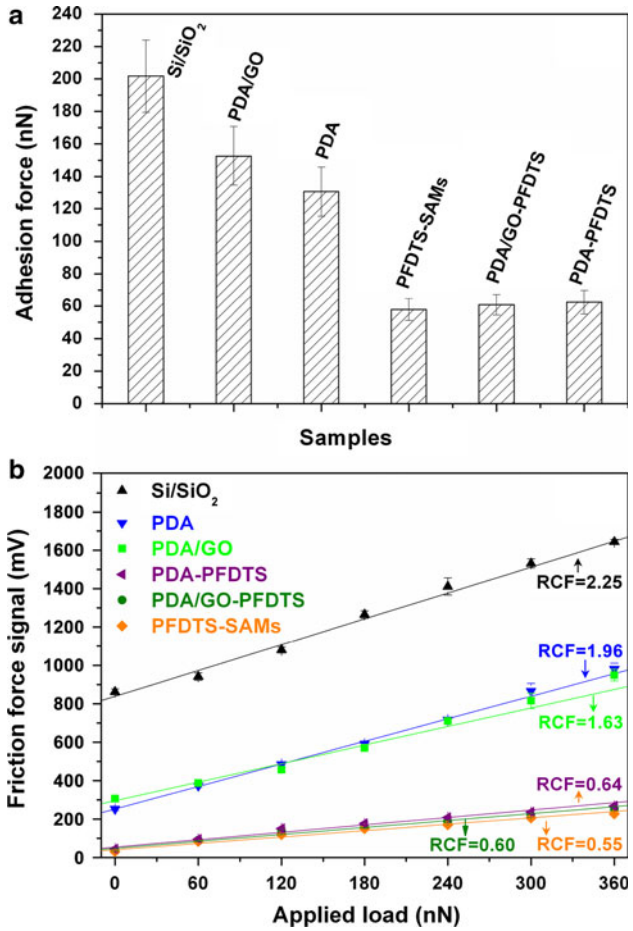

Fig. 6 Adhesive force (**a**) and friction-versus-load curves (**b**) for different samples

1.63 after deposition of PDA or PDA/GO, respectively. The RCF difference between PDA and PDA/GO suggests that the exposed GO sheets endow the sample with better nano-lubricating properties. After grafted with PFDTS, the samples (PFDTS-SAMs, PDA-PFDTS, and PDA/GO-PFDTS) become hydrophobic and the RCF values decrease to a relatively low level (in the range from 0.55 to 0.64). The excellent lubricity can be attributed to the hydrophobicity of the PFDTS outer layer, which can lower the interaction between the tip and film; consequently, the dissipation of the accumulated energy generated by the sliding of AFM tip on sample surface is smaller and a lower RCF is obtained. Besides, the low friction of the hydrophobic sample also can be ascribed to the nature of the PFDTS outer layer. Namely, the outer long chains have a significant freedom to swing and rearrange along the sliding direction under shear stress, and consequently yield a smaller resistance [32]. From above discussions, it can be seen that the RCF values of the hydrophobic samples are dependent on the microstructures of the PFDTS outer layer. Due to the tiny WCA difference as discussed in Sect. 3.1, it is assumed that PFDTS on bare Si substrate is packed more densely and consequently the RCF is the lowest.

The non-zero intercept, which is believed to be generated from the jump-to-contact instability caused by attractive forces during the approach of the tip to the sample surface, is the other important parameter to estimate the nano-tribological behaviors [33]. For the hydroxylated Si wafer, a highest intercept of 838 mV was observed, which decreases to 301 and 264 mV for the samples of PDA and PDA/GO, respectively. Once the sample becomes hydrophobic, the adhesive force between AFM tip and sample surface decreases and such jump gets weak. So, for the hydrophobic samples of PFDTS-SAMs, PDA-PFDTS, and PDA/GO-PFDTS, the intercept was 40.6, 54.7, and 47.6 mV, respectively.

3.3 Wear Resistance

In order to evaluate the wear resistance, the curves of friction coefficient-versus-sliding time for different samples obtained by a ball-on-plate tribometer are presented in Fig. 7. The PDA (Fig. 7a) exhibited high friction coefficient (0.29) and short anti-wear life (~50 s). After GO sheets were incorporated to form a multilayer film of PDA/GO (Fig. 7c), the anti-wear life increased sharply to ~2,850 s. Comparing the structure difference between PDA and PDA/GO, it is inferred that the interlayered GO sheets account for the excellent anti-wear performances. In other words, the nice lubricity of GO sheets (as proved in our recent works [7, 8]) and the nanocomposite structures lead to a lengthened anti-wear life. Once PFDTS was grafted onto PDA (Fig. 7b) or PDA/GO (Fig. 7d), the wear resistance was enhanced further; moreover, the friction coefficient decreased. These improvements were most likely to be related with the chemical composition and microstructures of the PFDTS outer layer. Specifically, owing to the high flexibility and low surface energy of the PFDTS outer layer, the friction coefficient for the multilayer decreases; moreover, the PFDTS monolayer possesses high elasticity and can endure larger stress, compression, and shear, without significant lateral displacement [34]. So, the wear resistance is correspondingly enhanced for the samples of PDA-PFDTS and PDA/GO-PFDTS. However, the lengthened anti-wear life for PDA/GO-PFDTS [>700 s, i.e., the difference between antiwear of PDA/GO-PFDTS (>3,600 s) and PDA/GO (~2,900 s)] is much longer than that of PDA-PFDTS [~100 s, i.e., the difference between antiwear of PDA-PFDTS (~150 s) and PDA (~50 s)] and anti-wear life of PFDTS-SAMs on bare Si substrate [several seconds, as shown in Fig. 7g]. In other words, the enhancement of PFDTS in wear resistance is sublayer dependent. Sublayer with better wear resistance endows the PFDTS outer layer with better enhancement.

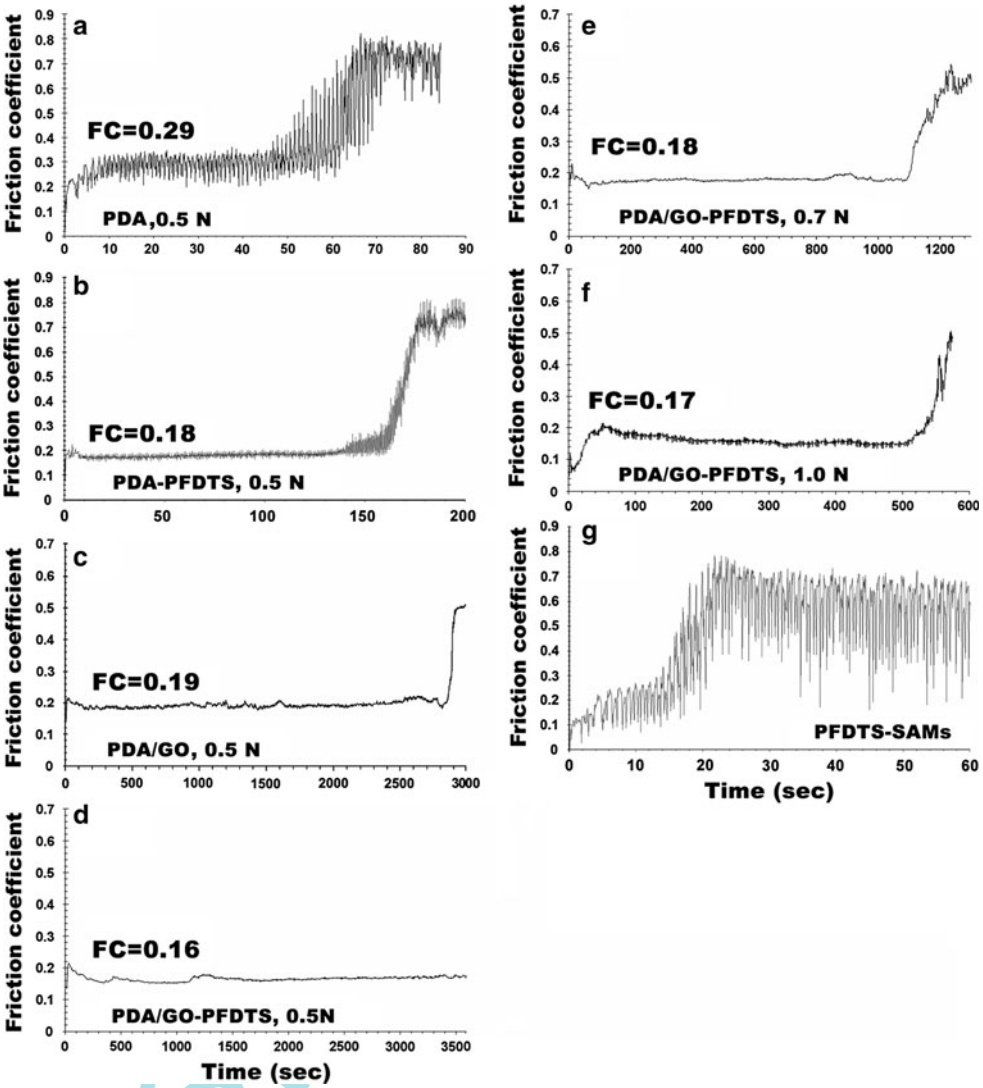

Fig. 7 Variation in friction coefficient with time for various samples at different applied load and a sliding frequency of 1 Hz: **a** PDA, 0.5 N; **b** PDA-PFDTS, 0.5 N; **c** PDA/GO, 0.5 N; **d** PDA/GO-PFDTS, 0.5 N; **e** PDA/GO-PFDTS, 0.7 N; **f** PDA/GO-PFDTS, 1.0 N; **g** PFDTS-SAMs, 0.5 N. The average friction coefficients before the friction coefficient increases sharply are marked near the curves

This is probably because the sublayer with better wear resistance can share larger stress, compression, and shear with the PFDTS outer layer during sliding, and consequently yields a better enhancement.

4 Conclusions

A hydrophobic multilayer abridged as PDA/GO-PFDTS was constructed on the silicon substrate by a process combining the non-electrostatic LBL assembly and chemografting. The microstructures and tribological behaviors were investigated. Results indicate that the multilayer possesses excellent tribological performances, i.e., high load affording capacity and low friction coefficient. The good friction reducing and wear resistance performances of such developed multilayer imply potential applications in NEMS/MEMS as lubricant coatings.

Acknowledgments The authors would like to thank the financial support from the Key Technology R&D Program (Grant No. 2010BGB00100) of Jiangxi Province, the Natural Science Foundation of Jiangxi Province (Grant No. 2010GZC0164), the International Science and Technology Cooperation Plan of Jiangxi Province (Grant No. 2010EHA01300), the National Science Foundation of Hangkong (Grant No. 2010ZE56012), and the Department of Education of Jiangxi Province (Grant Nos. GJJ11502; GJJ12422; GJJ12424).

References

1. Gómez-Navarro, C., Weitz, R.T., Bittner, A.M., Scolari, M., Mews, A., Burghard, M., Kern, K.: Electronic transport properties of individual chemically reduced graphene oxide sheets. Nano Lett. **7**, 3499–3503 (2007)
2. Geim, A.K.: Graphene: Status and Prospects. Science **324**, 1530–1534 (2009)
3. Wang, X., Zhi, L.J., Müllen, K.: Transparent, conductive graphene electrodes for dye-sensitized solar cells. Nano Lett. **8**, 323–327 (2008)

4. Gilje, S., Han, S., Wang, M.S., Wang, K.L., Kaner, R.B.: A chemical route to graphene for device applications. Nano Lett. **7**, 3394–3398 (2007)
5. Kim, Y.-K., Min, D.-H.: Durable large-area thin films of graphene/carbon nanotube double layers as a transparent electrode. Langmuir **25**, 11302–11306 (2009)
6. Wei, Z.Q., Barlow, D.E., Sheehan, P.E.: The assembly of single-layer graphene oxide and graphene using molecular templates. Nano Lett. **8**, 3141–3145 (2008)
7. Ou, J.F., Wang, J.Q., Liu, S., Mu, B., Ren, J.F., Wang, H.G., Yang, S.R.: Tribology study of reduced graphene oxide sheets on silicon substrate synthesized via covalent assembly. Langmuir **26**, 15830–15836 (2010)
8. Ou, J.F., Wang, Y., Wang, J.Q., Liu, S., Li, Z.P., Yang, S.R.: Self-assembly of octadecyltrichlorosilane on graphene oxide and the tribological performances of the resultant film. J. Phys. Chem. C. **115**, 10080–10086 (2011)
9. Stankovich, S., Dikin, D.A., Dommett, G.H.B., Kohlhaas, K.M., Zimney, E.J., Stach, E.A., Piner, R.D., Nguyen, S.T., Ruoff, R.S.: Graphene-based composite materials. Nature **442**, 282–286 (2006)
10. Lambert, T.N., Chavez, C.A., Hernandez–Sanchez, B., Lu, P., Bell, N.S., Ambrosini, A., Friedman, T., Boyle, T.J., Wheeler, D.R., Huber, D.L.: Synthesis and characterization of titania–graphene nanocomposites. J. Phys. Chem. C **113**, 19812–19823 (2009)
11. Park, S., An, J., Suk, J.W., Ruoff, R.S.: Graphene-based actuators. Small **6**, 210–212 (2010)
12. Chen, H.Q., Müller, M.B., Gilmore, K.J., Wallace, G.G., Li, D.: Mechanically strong, electrically conductive, and biocompatible graphene paper. Adv. Mater. **20**, 3557–3561 (2008)
13. Chen, C.M., Yang, Q.-H., Yang, Y.G., Lv, W., Wen, Y.F., Hou, P.-X., Wang, M.Z., Cheng, H.M.: Self-assembled free-standing graphite oxide membrane. Adv. Mater. **21**, 3007–3011 (2009)
14. Liu, S., Ou, J.F., Li, Z.P., Yang, S.R., Wang, J.Q.: Layer-by-layer assembly and tribological property of multilayer ultrathin films constructed by modified graphene sheets and polyethyleneimine. Appl. Surf. Sci. **258**, 2231–2236 (2012)
15. Li, Z.P., Wang, J.Q., Liu, X.H., Liu, S., Ou, J.F., Yang, S.R.: Electrostatic layer-by-layer self-assembly multilayer films based on graphene and manganese dioxide sheets as novel electrode materials for supercapacitors. J. Mater. Chem. **21**, 3397–3403 (2011)
16. Lee, H., Dellatore, S.M., Miller, W.M., Messersmith, P.B.: Mussel-inspired surface chemistry for multifunctional coatings. Science **318**, 426–430 (2007)
17. Kulkarni, D.D., Choi, I., Singamaneni, S.S., Tsukruk, V.V.: Graphene oxide-polyelectrolyte nanomembranes. ASC Nano **4**, 4667–4676 (2010)
18. Maboudian, R., Robert Ashurst, W., Carraro, C.: Tribological challenges in micromechanical systems. Tribol. Lett. **12**, 95–100 (2002)
19. Bourlinos, A.B., Gournis, D., Petridis, D., Szabó, T., Szeri, A., Dékány, I.: Graphite oxide: chemical reduction to graphite and surface modification with primary aliphatic amines and amino acids. Langmuir **19**, 6050–6055 (2003)
20. Dékány, I., Krüger-Grasser, R., Weiss, A.: Selective liquid sorption properties of hydrophobized graphite oxide nanostructures. Colloid Polym. Sci. **276**, 570–576 (1998)
21. Lerf, A., He, H., Forster, M., Klinowski, J.: Structure of graphite oxide revisited. J. Phys. Chem. B **102**, 4477–4482 (1998)
22. Yang, H., Li, F., Shan, C., Han, D., Zhang, Q., Niu, L., Ivaska, A.: Covalent functionalization of chemically converted graphene sheets via silane and its reinforcement. J. Mater. Chem. **19**, 4632–4638 (2009)
23. Patz, T., Cristescu, R., Narayan, R., Menegazzo, N., Mizaikoff, B., Messersmith, P.B., Stamatin, I., Mihailescu, I.N., Chrisey, D.B.: Processing of mussel-adhesive protein analog copolymer thin films by matrix-assisted pulsed laser evaporation. Appl. Surf. Sci. **248**, 416–421 (2005)
24. Chen, S.G., Chen, Y., Lei, Y.H., Yin, Y.S.: Novel strategy in enhancing stability and corrosion resistance for hydrophobic functional films on copper surfaces. Electrochem. Commun. **11**, 1675–1679 (2009)
25. Fan, X., Lin, L., Dalsin, J.L., Messersmith, P.B.: Biomimetic anchor for surface-initiated polymerization from metal substrates. J. Am. Chem. Soc. **127**, 15843–15847 (2005)
26. Pan, F., Jia, H., Qiao, S., Jiang, Z., Wang, J., Wang, B., Zhong, Y.J.: Bioinspired fabrication of high performance composite membranes with ultrathin defect-free skin layer. Membrane Sci. **341**, 279–285 (2009)
27. Yang, D.X., Velamakanni, A., Bozoklu, G., Park, S., Stoller, M., Piner, R.D., Stankovich, S., Jung, I., Field, D.A., Ventrice Jr, C.A., Ruoff, R.S.: Chemical analysis of graphene oxide films after heat and chemical treatments by X-ray photoelectron and Micro-Raman spectroscopy. Carbon **47**, 145–152 (2009)
28. Mo, Y.F., Zhu, M., Bai, M.W.: Preparation and nano/microtribological properties of perfluorododecanoic acid (PFDA)–3-aminopropyltriethoxysilane (APS) self-assembled dual-layer film deposited on silicon. Colloids Surf A: PhysIcochem. Eng. Aspects **322**, 170–176 (2008)
29. Ou, J.F., Wang, J.Q., Liu, S., Zhou, J.F., Ren, S.L., Yang, S.R.: Microtribological and electrochemical corrosion behaviors of polydopamine coating on APTS-SAM modified Si substrate. Appl. Surf. Sci. **256**, 894–899 (2009)
30. Ou, J.F., Wang, J.Q., Qiu, Y.N., Liu, L.Z., Yang, S.R.: Mechanical property and corrosion resistance of zirconia/polydopamine nanocomposite multilayer films fabricated via a novel non-electrostatic layer-by-layer assembly technique. Surf. Interface Anal. **43**, 803–808 (2011)
31. Chandross, M., Lorenz, C.D., Grest, G.S., Stevens, M.J., Webb, E.B.: Nanotribology of anti-friction coatings in MEMS. JOM-J. Min. Met. Mater. Soc. **57**, 55–61 (2005)
32. Ren, S.L., Yang, S.R., Wang, J.Q., Liu, W.M., Zhao, Y.P.: Preparation and tribological studies of stearic acid self-assembled monolayers on polymer-coated silicon surface. Chem. Mater. **16**, 428–434 (2004)
33. Tsukruk, V.V., Bliznyuk, V.N.: Adhesive and friction forces between chemically modified silicon and silicon nitride surfaces. Langmuir **14**, 446–455 (1998)
34. Houston, J.E., Kim, H.I.: Adhesion, friction, and mechanical properties of functionalized alkanethiol self-assembled monolayers Acc. Chem. Res. **35**, 547–553 (2002)